Recibido: 05/04/2025
Aceptado: 17/09/2025
Disponible en línea: 21/10/2025
Publicado: 31/01/2026

REVISTA DE TELEDETECCIÓN
Asociación Española de Teledetección
(2026) 67, 23671
ISSN 1133-0953
EISSN 1988-8740
https://doi.org/10.4995/raet.2026.23671

Estimation of water stress in maize cultivation utilizing thermal and multispectral imaging from UAVs with machine learning algorithms in Lambayeque, Peru

Camila Cruz-Grimaldo*[1], Cesar Vilca-Gamarra[1], José Millan-Ramírez[1], Sheyla Y. Chumbimune-Vivanco[1], Cristina Llanos-Carrillo[1], Elvis Vera[1], Alex Agurto[1], Javier Quille-Mamani[2], Hairo León[1]

[1] *National Institute for Agrarian Innovation (INIA), Directorate of Research and Technological Development, Av. La Molina, 1981 Lima, Peru.*

[2] *Geo-Environmental Cartography and Remote Sensing Group (CGAT), Universitat Politècnica de València, Camí de Vera s/n, 46022 Valencia, Spain.*

Abstract: Maize (*Zea mays* L.) is a fundamental cereal in global food security, but its vulnerability to water stress compromises its productivity and threatens food availability. This study analyzed the relationship between the crop water stress index (CWSI), obtained from thermal images captured by the Zenmuse H20T camera, and various vegetation indices derived from the MicaSense RedEdge-MX Dual. The analysis included machine learning (ML) models such as random forest (RF), k-nearest neighbors (KNN), and gradient boosting regression (GBR). The results showed that RF was the most accurate model for predicting CWSI in maize, with a coefficient of determination (R^2) of 0.80, a root mean square error (RMSE) of 0.13, and a mean absolute error (MAE) of 0.09. KNN achieved an R^2 of 0.78, an RMSE of 0.13, and an MAE of 0.09, while GBR reached an R^2 of 0.79, an RMSE of 0.14, and an MAE of 0.10. The red band (668 nm) played a crucial role in RF (70.69%) and GBR (50.92%), whereas in KNN, the simple ratio (SR) index showed the highest importance (36.40%). These findings confirm the superiority of ML models over traditional regression approaches for estimating CWSI in maize. Despite the satisfactory results, the algorithms underestimated CWSI values derived from thermal images, which highlights the need to refine these models to improve their accuracy in future agricultural applications.

Key words: crop water stress index (CWSI), machine learning, precision agriculture, thermal image, Vegetation Index.

Estimación del estrés hídrico en el cultivo de maíz utilizando imágenes térmicas y multiespectrales obtenidas de un RPA y algoritmos de aprendizaje automático en Lambayeque, Perú

Resumen: El maíz (*Zea mays* L.) es un cereal fundamental en la seguridad alimentaria global, pero su vulnerabilidad al estrés hídrico compromete su productividad y amenaza la disponibilidad de alimentos. Este estudio analizó la relación entre el índice de estrés hídrico de los cultivos (CWSI), obtenido a partir de imágenes térmicas captadas por la cámara Zenmuse H20T, y diversos índices de vegetación derivados de la MicaSense RedEdge-MX Dual. El análisis incluyó modelos de aprendizaje automático (ML) como *random forest* (RF), *k-nearest neighbors* (KNN) y

To cite this article: Cruz-Grimaldo, C., Vilca-Gamarra, C., Millan-Ramírez, J., Chumbimune-Vivanco, S.Y., Llanos-Carrillo, C., Vera, E., Agurto, A., Quille-Mamani, J., León, H. 2025. Estimation of water stress in maize cultivation utilizing thermal and multispectral imaging from UAVs with machine learning algorithms in Lambayeque, Peru. *Revista de Teledetección*, *67*, e23671. https://doi.org/10.4995/raet.2026.23671

* *Corresponding author: camila.cruz239@gmail.com*

gradient boosting regression (GBR). Los resultados mostraron que RF fue el modelo más preciso para predecir el CWSI en el maíz, con un coeficiente de determinación (R^2) de 0,80, un error cuadrático medio (RMSE) de 0,13 y un error absoluto medio (MAE) de 0,09. KNN alcanzó un R^2 de 0,78, un RMSE de 0,13 y un MAE de 0,09, mientras que GBR obtuvo un R^2 de 0,79, un RMSE de 0,14 y un MAE de 0,10. La banda roja (668 nm) tuvo un papel crucial en RF (70,69 %) y GBR (50,92 %), mientras que en KNN el índice de proporción simple (SR) presentó la mayor importancia (36,40 %). Estos hallazgos confirman la superioridad de los modelos de ML sobre los enfoques de regresión tradicionales para estimar el CWSI en el maíz. A pesar de los resultados satisfactorios, los algoritmos subestimaron los valores del CWSI obtenidos a partir de imágenes térmicas, lo que resalta la necesidad de optimizar estos modelos para mejorar su precisión en futuras aplicaciones agrícolas.

Palabras clave: índice de estrés hídrico de los cultivos (CWSI), aprendizaje automático, agricultura de precisión, imagen térmica, índice de vegetación.

1. Introduction

Maize (*Zea mays* L.) is one of the most significant crops globally, contributing approximately 20% of the world's caloric intake (Waqas *et al.*, 2021). However, maize yield rates have exhibited a deceleration since the 1960s (Long and Ort, 2010), and current projections fall short of meeting future demands, posing a threat to food security (Ummenhofer and Meehl, 2017). This slowdown is largely attributed to temperature variability during the crop's phenological cycle, adversely affecting plant growth and development as well as associated ecosystem services (Zafar *et al.*, 2018). As a thermophilic plant, maize is particularly susceptible to thermal stress when temperatures exceed 30 °C, leading to reduced grain yields if such stress persists over extended periods (Schauberger *et al.*, 2017).

Water scarcity represents one of the foremost challenges in water management, particularly in arid and semi-arid regions (Zhang *et al.*, 2019). This issue has intensified due to rising temperatures associated with climate change, which diminishes water availability for agricultural use (Jin *et al.*, 2018). In this context, estimating water stress has become crucial for optimizing water utilization in agricultural activities (Han *et al.*, 2016). Although traditional methods based on soil moisture content, stomatal behavior, and physiological characteristics (Zhang *et al.*, 2019) have been employed, measuring these parameters is labor-intensive, costly, and time-consuming (Li *et al.*, 2010). Consequently, the use of indirect methods for assessing water status has gained prominence. These methods utilize canopy temperature as an indicator of water stress, based on its inverse relationship with water loss rates and stomatal behavior (Berni *et al.*, 2009). In this context, studies conducted by Jackson *et al.* (1981) and Jackson *et al.* (1977) demonstrated that the difference between canopy temperature and air temperature, combined with environmental variables such as vapor pressure deficit and net radiation, can be used to calculate a quantitative crop water stress index. This index, known as the Crop Water Stress Index (CWSI), reflects the relationship between actual and potential evapotranspiration.

Remote sensing technologies significantly reduce the need for labor-intensive techniques and time-consuming methods traditionally used to detect water stress (Pradawet *et al.*, 2022). Remote sensors facilitate timely, non-destructive measurements of canopy temperature with lower personnel demands (Ihuoma and Madramootoo, 2017). Water stress estimation is achieved through the normalized crop water stress index (CWSI), developed to account for environmental parameters that may significantly alter the relationship between plant stress and its temperature (Pradawet *et al.*, 2022), with calculations based on canopy surface temperature (Poblete-Echeverría *et al.*, 2018). Literature indicates that the CWSI serves as a reliable indicator of water stress across various crops, including maize (Kapari *et al.*, 2024), chili peppers (Duran *et al.*, 2021), and potatoes (Ekinzog *et al.*, 2022). However, obtaining CWSI through thermal infrared (TIR) bands presents practical challenges, such as the higher cost of sensors, lower spatial resolution compared to multispectral sensors, and the need to calibrate emissivity (Kapari *et al.*, 2025). While both thermal and optical bands require atmospheric correction, with thermal data processing being simpler in

some cases, vegetation indices derived from multispectral data remain valuable for detecting subtle changes in the canopy (Giovos *et al.*, 2021). Various studies, such as those by Baluja *et al.* (2012), report a correlation value of 0.68 between NDVI and CWSI, while Zarco-Tejada *et al.* (2013) obtained satisfactory R^2 values of 0.77 between the normalized photochemical reflectance index (PRInorm) and CWSI. To establish such correlations, sophisticated statistical techniques are required, including machine learning methods (Alabi *et al.*, 2022). For instance, the random forest algorithm has optimally estimated CWSI in *Brassica chinensis* cultivation (Yang *et al.*, 2021), while Ma *et al.* (2021) identified promising results for support vector machine algorithms in predicting water content with optimal R^2 values of 0.72 and root mean square error (RMSE) values of 6.22%.

This study investigates the estimation of crop water stress index (CWSI) using multispectral data. Although CWSI can be derived directly from thermal data, its acquisition is often less frequent, more costly, and has a lower spatial resolution compared to multispectral sensors. Therefore, the objective is to evaluate the potential of vegetation indices (VIs) as proxies for water stress estimation, allowing for more accessible and frequent monitoring. The adoption of this technology responds to the need for accurate and timely information to support efficient water resource management in agricultural systems. An experimental plot was established with different irrigation levels to ensure a wide range of water stress conditions. The main objective is to establish a baseline knowledge of water stress dynamics in maize crops under the prevailing climatic conditions on the northern coast of Peru, in particular in the Lambayeque region, where water availability is increasingly threatened by climate variability. The results are expected to provide valuable information for local decision-making, support the development of sustainable regional water management strategies and serve as a basis for future research. Furthermore, the integration of remote sensing tools with precision agriculture techniques offers a promising avenue for optimising water use in agriculture.

2. Materials and Methods

2.1. Study area

The research was conducted over a usable area of 0.4 ha, located in Lot 2-1 of the Vista Florida Agricultural Experimental Station, district of Picsi, Lambayeque region, Peru (Figure 1). The average altitude of the site is 40 m a.s.l., characterized by a predominantly temperate arid climate. The crop under study was yellow dent corn (YDC; *Zea mays* L.) 'INIA 619-MEGA HYBRID', cultivated using a drip irrigation system. The planting framework consisted of 0.30 m between plants and 0.75 m between irrigation tapes, with a planting depth ranging from 3 to 5 cm.

The study was conducted using a completely randomized block design (CRBD) with four blocks and four replicates per block. Three irrigation treatments corresponded to 25%, 50%, and 75% of crop water requirements were evaluated, along with a fully irrigated control. These percentages were calculated based on crop coefficients (Kc) provided in FAO56 guidelines. During the study period, minimum and maximum temperatures were recorded as 12.2 and 33.1 °C, respectively, with a maximum relative humidity of 81.7% and a total precipitation of 3.6 mm (Figure 2). These data were provided by the automatic weather station "Vista Florida" operated by the National Service of Meteorology and Hydrology of Peru (SENAMHI).

2.2. Acquisition of thermal and multispectral information

A total of five unmanned aerial vehicle (UAV) flights was carried out during the crop cycle at 35, 48, 58, 63 and 99 DAS, covering both vegetative and reproductive phases. Aerial images were acquired between 11 am and 1 pm (UTC-5) under clear sky conditions. A quadcopter-type unmanned aerial vehicle (UAV), the Matrice 300 RTK (DJI, Shenzhen, China), was used for monitoring. This UAV has a battery with a maximum autonomy of 40 minutes. The UAV was equipped with the Zenmuse H20T payload (DJI, Shenzhen, China) to capture thermal and RGB images (Figure 3a) and the Dual RedEdge+Blue MicaSense camera (MicaSense Inc., Seattle, Washington, USA) for capturing multispectral images, which were

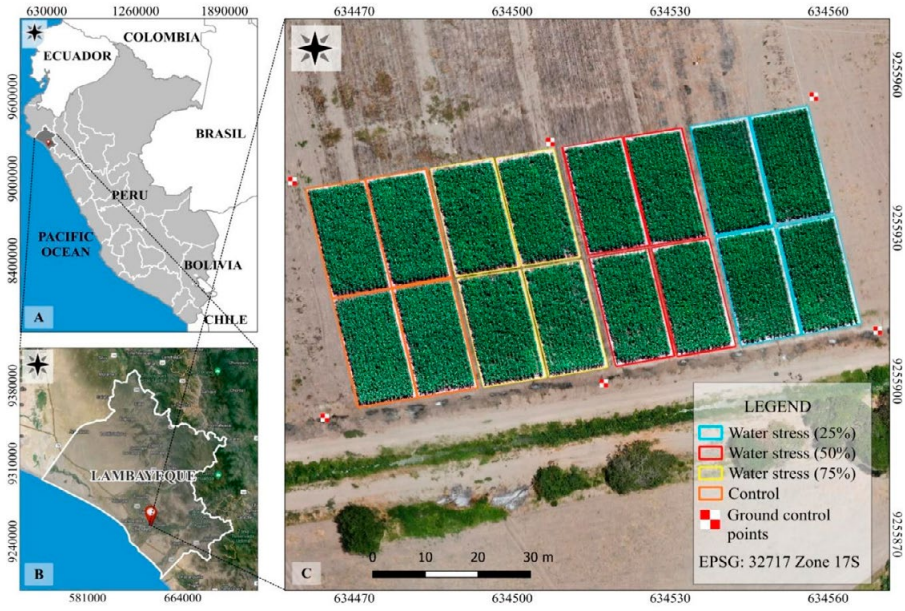

Figure 1. Study Area Location: (A) Location of the study area on the northern coast of Peru. (B) Satellite image of the Lambayeque department. (C) Distribution of the research plot with its respective treatments. The reference system is EPSG: 32717. The image was obtained from UAV flights.

calibrated before each flight using the AIRNOV reflectance panel (Figure 3c). The multispectral camera captures images synchronously across ten spectral bands (Table 1) and stores them as separate image files. Additionally, the images were geo-tagged with the assistance of a global navigation satellite system (GNSS) receiver mounted on top of the UAV, provided by the camera manufacturer.

The thermal camera (Zenmuse H20T; DJI, Shenzhen, China) (Figure 3d), features a 58 mm lens and operates at a frequency of 30 Hz to record temperature measurements within a

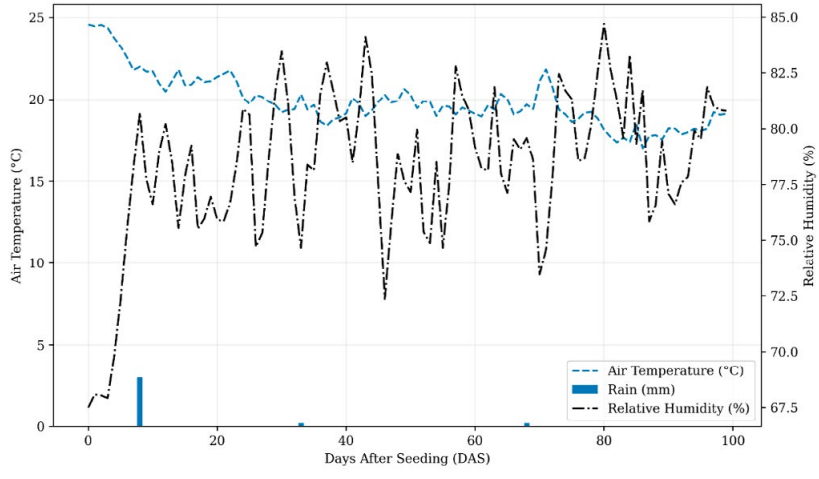

Figure 2. Climatic conditions during the study period.

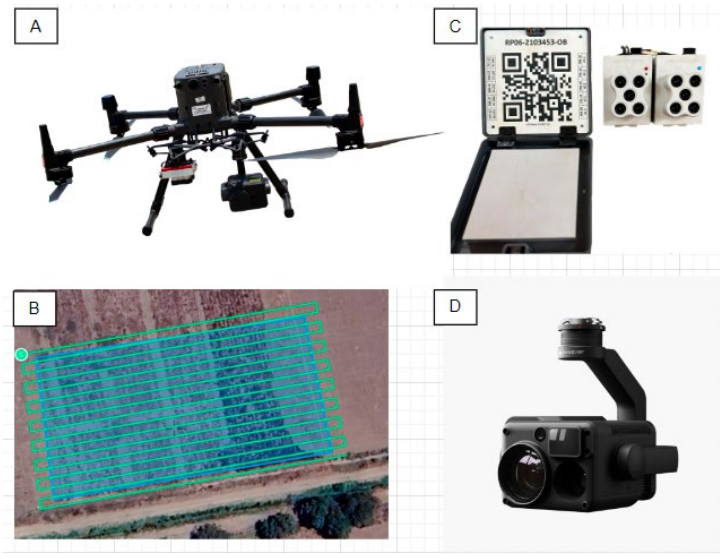

Figure 3. (A) UAV system DJI Matrice 300, (B) DJI M-300 flight plan, (C) MicaSense Dual RedEdge+Blue and reflectance panel, and (D) thermal camera Zenmuse H20T.

range of 8-14 µm, with a thermal resolution of 640 × 512 pixels, and an accuracy of ±2 °C or ±2%, measured at 25 °C from a black body at 5 m in laboratory conditions. Flights were conducted using the DJI Pilot 2 application (Figure 3b) at an altitude of 30 m above ground level, with front and lateral overlaps of 75/80, 80/80, and 75/80 for the multispectral, thermal, and RGB cameras respectively.

Table 1. Wavelengths and bandwidth of the MicaSense Dual RedEdge+Blue camera system.

	Centre wavelength	Bandwidth
Band names	nm	nm
Blue 444	444	28
Blue 475	475	32
Green 531	531	14
Green 560	560	27
Red 650	650	16
Red 668	668	14
RE 705	705	10
RE 717	717	12
RE 749	740	18
NIR 840	842	57

The calibration of thermal images was performed using data obtained from a handheld infrared radiometer (Apogee MI-210; Apogee Instruments, Utah, USA), over four surfaces: Aluminum foil, bare agricultural soil, black fabric, and white fabric, which were framed within a PVC square (1 m²). Measurements were taken at a height of 40 cm above the surface (Figure 4), collecting information prior to each UAV monitoring session. In total, 36 readings were recorded per surface, resulting in 144 readings per flight and a cumulative total of 720 readings throughout the research development.

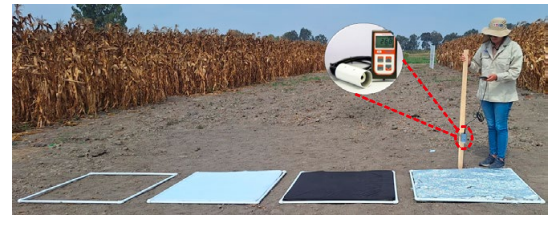

Figure 4. Data collection of temperature on surfaces: aluminum, black fabric, white fabric, and bare soil, using the handheld infrared radiometer.

The generation of orthomosaics was carried out using Pix4D Mapper software (Pix4D S.A., Prilly, Switzerland), following the three procedures described by Del Río *et al.* (2020): Photo alignment, generation of a point cloud, and production of orthomosaics. The software includes specific templates for generating mosaics from RGB, multispectral, thermal images, and 3D models, thanks to its camera model registration,

which allows it to recognize and process the formats of the captured images. Given that the flight was conducted at low altitude, it was not necessary to apply atmospheric correction to the optical bands. At such altitudes, atmospheric effects are minimal and can be ignored without compromising data quality. Accordingly, Daniels *et al.* (2023) state that this type of correction is not pertinent when working below 100 meters of altitude. The generated orthomosaics have a resolution of 0.05 cm pixel^{-1}. For georeferencing, five photogrammetric control points were placed in the field, identified with black and white colors. In the black sector, aluminum foil was used to facilitate the identification of control points in the thermal band (Figure 5).

2.3. Selection of vegetation indices

From the multispectral orthomosaics, vegetation indices (VIs) were calculated, which are detailed in Table 2. These selected indices are commonly used to relate the physiological parameters of the canopy, according to the study conducted by Pradawet *et al.* (2022). Additionally, VIs aims to enhance the optical characteristics of vegetation. Consequently, VIs are applied individually or in combination to minimize factors such as background noise from soils, especially in the initial days after sowing.

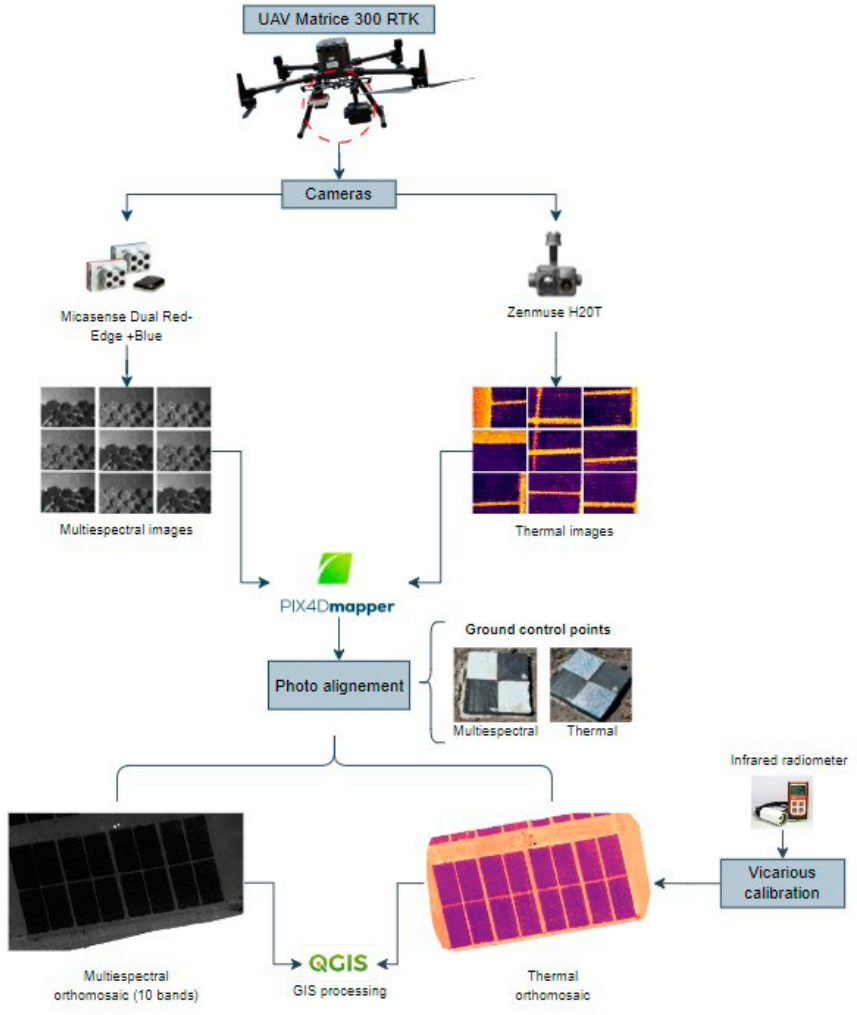

Figure 5. Flowchart of photogrammetric processing.

Table 2. List of vegetation indices (VIs) used to estimate the crop water stress index.

Vegetation indices	Equation	Sources
Normalized difference vegetation index (NDVI)	$\frac{\mathrm{NIR}_{842}-\mathrm{RED}_{(650,668)}}{\mathrm{NIR}_{842}+\mathrm{RED}_{(650,668)}}$	Peñuelas *et al.* (1993)
Green normalized difference vegetation index (GNDVI)	$\frac{\mathrm{NIR}_{842}-\mathrm{GREEN}_{(531,560)}}{\mathrm{NIR}_{842}+\mathrm{GREEN}_{(531,560)}}$	Gitelson *et al.* (1996)
Normalized difference red edge index (NDRE)	$\frac{\mathrm{NIR}_{842}-\mathrm{RED\ EDGE}_{(705,717,740)}}{\mathrm{NIR}_{842}+\mathrm{RED\ EDGE}_{(705,717,740)}}$	Gitelson and Merzlyak (1994)
Soil adjusted vegetation index (SAVI)	$\left(\frac{\mathrm{NIR}_{842}-\mathrm{RED}_{(650,668)}}{\mathrm{NIR}_{842}+\mathrm{RED}_{(650,668)}+L}\right)\times\left(1+L\right)$ L is a constant between 0 and 1	Huete (1988)
Optimized soil-adjusted vegetation index (OSAVI)	$\frac{\mathrm{NIR}_{842}-\mathrm{RED}_{(650,668)}}{\mathrm{NIR}_{842}+\mathrm{RED}_{(650,668)}+0.16}$	Xue and Su (2017)
Green chlorophyll index (CI_green)	$\frac{\mathrm{NIR}_{842}}{\mathrm{GREEN}_{(531,560)}}-1$	Zhang and Zhou (2015)
Red edge chlorophyll index (CIRE)	$\frac{\mathrm{NIR}_{842}}{\mathrm{RED\ EDGE}_{(705,717,740)}}-1$	Gitelson and Merzlyak (1994)
Red edge NDVI (RENDVI)	$\frac{\mathrm{NIR}_{842}-\mathrm{RED\ EDGE}_{(705,717,740)}}{\mathrm{NIR}_{842}+\mathrm{RED\ EDGE}_{(705,717,740)}}$	Bannari *et al.* (1995)
Simple ratio (SR)	$\frac{\mathrm{NIR}_{842}}{\mathrm{RED}_{(650,668)}}$	Baret and Guyot (1991)
Canopy chlorophyll content index (CCCI)	$\frac{\mathrm{NDRE}}{\mathrm{NDVI}}$	Varco *et al.* (2013)
MERIS terrestrial chlorophyll index (MTCI)	$\frac{\mathrm{NIR}_{842}-\mathrm{RED\ EDGE}_{(705,717,740)}}{\mathrm{RED\ EDGE}_{(705,717,740)}-\mathrm{RED}_{668}}$	Dash and Curran (2004)
Normalized difference water index (NDWI)	$\frac{\mathrm{GREEN}_{(531,560)}-\mathrm{NIR}_{842}}{\mathrm{GREEN}_{(531,560)}+\mathrm{NIR}_{842}}$	Özelkan (2020)
Ratio vegetation index (RVI)	$\frac{\mathrm{RED}_{(650,668)}}{\mathrm{NIR}_{842}}$	Feng *et al.* (2020)
Transformed chlorophyll absorption in reflectance index (TCARI) $\frac{3\left[\mathrm{RED\ EDGE}_{(705,717,740)}-\mathrm{RED}_{(650,668)}-0.2\left(\mathrm{RED\ EDGE}_{(705,717,740)}-\mathrm{GREEN}_{(531,560)}\right)\left(\frac{\mathrm{RED\ EDGE}_{(705,717,740)}}{\mathrm{RED}_{(650,668)}}\right)\right]}{\mathrm{OSAVI}}$		Haboudane *et al.* (2002)
Photochemical reflectance index (PRI)	$\frac{\mathrm{GREEN}_{531}-\mathrm{GREEN}_{560}}{\mathrm{GREEN}_{531}-\mathrm{GREEN}_{560}}$	Gamon *et al.* (1997)
Canopy chlorophyll content index (CCI)	$\frac{\mathrm{GREEN}_{531}-\mathrm{RED}_{650}}{\mathrm{GREEN}_{531}+\mathrm{RED}_{650}}$	El-Shikha *et al.* (2008)

2.4. Crop water stress index (CWSI)

The CWSI is associated with the cooling of the leaf canopy during the transpiration process; when soil moisture in the root zone decreases, leaf temperature increases. Consequently, transpiration and stomatal conductance are reduced (Elsherbiny *et al.*, 2021). CWSI was calculated using thermal orthomosaics of the crop calibrated with a handheld infrared radiometer. The CWSI was computed using the Equation 1 proposed by Jones and Leinonen (2003):

$$CWSI = \frac{T_c - T_{wet}}{T_{dry} - T_{wet}} \quad (1)$$

Where *Tc* is the canopy temperature measured with thermal camera, T_{wet} is the reference temperature of a fully transpiring (well-watered) canopy, and T_{dry} is the reference temperature of a non-transpiring (fully water-stressed) canopy.

The wet reference temperature (T_{wet}) was estimated as the canopy temperature measured between 07:00 and 08:00 h, immediately after irrigation, when the crop reaches maximum leaf water

potential and canopy temperature equilibrates with the surrounding air. This condition represents a fully transpiring canopy, consistent with the definition of wet reference surfaces described by Idso *et al.* (1981) and Jones (1999). Under Peruvian coastal conditions, Villar *et al.* (2021) applied this methodology using thermocouple measurements in rice crops during the growing season, which provided a practical basis for the study. Various approaches have been developed to estimate the CWSI, spanning from empirical techniques to physically based modeling strategies. Among these are: (i) empirical procedures grounded in field measurements, (ii) methods built upon surface energy balance principles, and (iii) the direct method, also referred to as the Idso approach, which was implemented in the present work (Maes & Steppe, 2012). The direct method offers distinct advantages for thermal remote sensing, as it demands fewer meteorological and surface inputs compared to physically based alternatives. This makes it especially useful when detailed environmental data are lacking, and it has shown strong performance in capturing spatial variability of crop water stress in semi-arid agricultural systems. The CWSI value ranges from 0 to 1, with a value close to 0 indicating the absence of water stress (well-watered plant), and a value close to 1 representing the maximum level of water stress (Kapari *et al.*, 2025).

2.5. Data modeling and evaluation

2.5.1. Machine learning models

Variables were pre-filtered based on their Spearman correlation strength ($|r| > 0.7$) and Variance Inflation Factor ($VIF < 5$) to reduce multicollinearity, narrowing the initial 46 variables down to 23 using the SciPy library (Virtanen *et al.*, 2020). The dataset was split into 70% for calibration (training) and 30% for validation (testing) using a randomized stratified approach to ensure representative distribution of stress levels in both subsets. We evaluated multiple machine learning algorithms to mitigate bias in model selection using Scikit-learn (sklearn) library (Kramer, 2016):

- Simple Linear Regression (using the highest-correlated variable, RVI),
- Multiple Linear Regression,
- Regularized models (Ridge and Lasso regression),
- Ensemble methods (Random Forest, Gradient Boosting Regressor),
- k-Nearest Neighbors (KNN),
- Support Vector Machines (SVM), and
- Artificial Neural Networks (ANN).

To prevent overfitting, the following strategies were implemented: Regularization: in the Ridge and Lasso models, L2 and L1 penalties were applied, respectively, which restrict the magnitude of the model coefficients to avoid overly complex solutions (Hastie *et al.*, 2001).

Hyperparameter optimization: an exhaustive search (grid search) with k-fold cross-validation (k=5) was performed to systematically adjust the key hyperparameters of each algorithm (e.g., maximum depth in RF, learning rate in GBR), ensuring that the selected configurations generalized better to unseen data (Feurer *et al.*, 2015).

Early stopping: iterative models (e.g., ANN, GBR), early stopping was implemented by monitoring the loss in the validation set to stop training when no improvements were observed (Ying, 2019).

Stratified division: stratified random partitioning ensured that both sets (training/validation) maintained similar proportions of the target variable, avoiding biases in performance evaluation.

2.5.2. Model performance evaluation

The statistical analysis was conducted in the Python programming environment (version 3.10.13), utilizing Google Colab (Jupyter Notebook) for hosting. Open-source packages such as Pandas and NumPy were employed for database management and to perform various statistical tests among the spectral bands, VIs, and CWSI. We used the coefficient of determination (R^2), Root Mean Square Error (RMSE) and Mean Absolute Error (MAE) in this study, as these metrics are commonly employed to evaluate the prediction performance of machine learning

models. The mathematical formulations are presented in Equations 2, 3, and 4, respectively.

$$R^2 = 1 - \frac{\sum_{i=1}^{n} \left(y_i - \hat{y}_i\right)^2}{\sum_{i=1}^{n} \left(y_i - \bar{y}\right)^2} \quad (2)$$

$$\mathrm{MAE} = \frac{\sum_{i=1}^{n} \left|y_i - \hat{y}_i\right|}{n} \quad (3)$$

$$\mathrm{RMSE} = \sqrt{\frac{\sum_{i=1}^{n} \left(y_i - \hat{y}_i\right)^2}{n}} \quad (4)$$

In Equations 2–4, y, $\hat{y}$, and $\bar{y}$ are the observed, predicted, and observed mean CWSI values of the plot i, and n is the total number of samples within the study area.

3. Results and discussion

3.1. Correction of thermal images

The linear relationship between the temperature values recorded by the H20T thermal camera and the handheld infrared radiometer, evaluated across four different surfaces, was analyzed under the same environmental conditions of the study area on each monitoring date (Figure 6). For each date, the coefficient of determination (R^2) was calculated, yielding a range of 0.97 to 0.99. Furthermore, a general equation was obtained: $y = 0.6932x + 11.753$, with an R^2 of 0.97 and a Pearson coefficient (r) of 0.98, indicating a high reliability in the use of temperature data provided by the H20T thermal camera for this specific study area.

3.2. Estimation of the crop water stress index (CWSI)

Figure 7 presents the values of the crop water stress index (CWSI) obtained during five monitoring dates throughout the maize vegetative cycle, categorized by treatment. The highest average CWSI value was recorded at 99 days after sowing (DAS) (0.45 ± 0.14) in the treatment with 25% irrigation, while the lowest average value was observed at 63 DAS (0.19 ± 0.12) in the control treatment. Water stress increased as maize growth progressed, as the crop demands a greater amount of water during the maturation phase (Song *et al.*, 2019; Wang *et al.*, 2023).

In addition, as shown in Figure 7, the average results indicated that water stress was moderate (CWSI < 0.4), except for the treatment with 25% irrigation at 99 DAS, where a CWSI of 0.45 ± 0.14 was observed. Additionally, at 35 DAS, the treatment with 75% irrigation exhibited the highest level of water stress, reflected in the range of values in the box plot (0.44 ± 0.24), which was attributed to a failure in the operation of the drip irrigation system. According to Jamshidi *et al.*

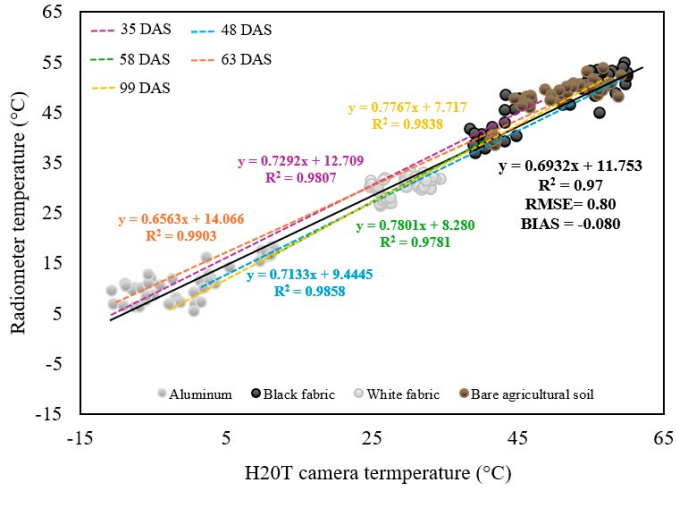

Figure 6. Relationship between temperatures recorded by the Apogee MI-210 radiometer and the Zenmuse H20T thermal camera.

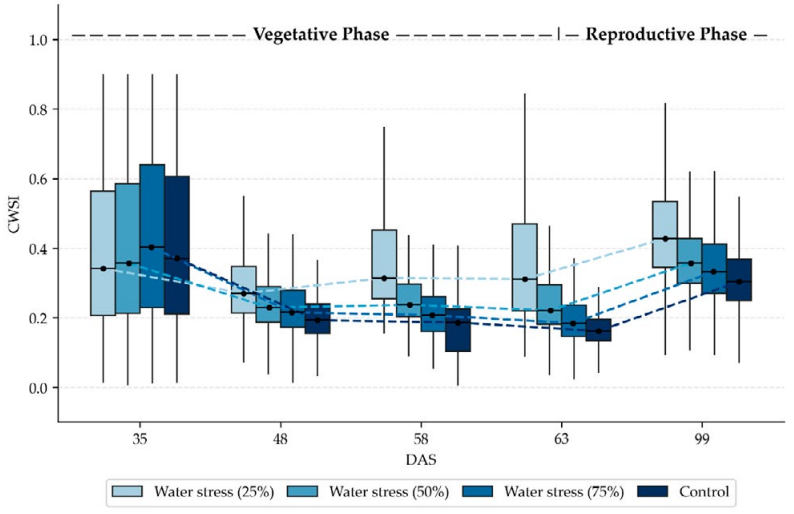

Figure 7. Crop water stress index (CWSI) during the vegetative period of maize.

(2020), values exceeding 0.40 in water stress negatively affect crop yield; however, in this study, the aim of the treatments was to achieve maximum variability in the data to develop a more reliable model.

3.3. Relationship between CWSI and spectral variables

Table 3 presents the Spearman correlation coefficients between the Crop Water Stress Index

Table 3. Spearman correlation coefficients between CWSI, spectral bands, and vegetation indices (VIs).

Vegetation index	Spearman correlation	Vegetation index	Spearman correlation	Spectral bands	Spearman correlation
$NDVI_{650}$	-0.78	$RENDVI_{740}$	-0.51	$Blue_{444}$	0.61
$NDVI_{668}$	-0.79	SR_{650}	-0.78	$Blue_{475}$	0.62
$GNDVI_{531}$	-0.74	SR_{668}	-0.79	NIR_{842}	-0.55
$GNDVI_{560}$	-0.78	$CCCI_{Rx}$	-0.43	$RedEdge_{705}$	0.61
$NDRE_{705}$	-0.76	$CCCI_{Rb,705}$	-0.49	$RedEdge_{717}$	0.31
$NDRE_{717}$	-0.77	$CCCI_{Rb,740}$	0.02	$RedEdge_{740}$	-0.43
$NDRE_{740}$	-0.51	MTCI	-0.61	Red_{650}	0.68
$SAVI_{650}$	-0.71	$MTCI_{Rb,705}$	-0.59	Red_{668}	0.72
$SAVI_{668}$	-0.72	$MTCI_{Rb,740}$	-0.10	$Green_{531}$	0.51
$OSAVI_{650}$	-0.74	$NDWI_{Rx}$	0.78	$Green_{560}$	0.44
$OSAVI_{668}$	-0.75	$NDWI_{Rb}$	0.78		
$CIgreen_{531}$	-0.74	RVI_{Rx}	0.79		
$CIgreen_{560}$	-0.78	RVI_{Rb}	0.79		
$CIRE_{705}$	-0.76	$TCARI_{Rx}$	-0.41		
$CIRE_{717}$	-0.77	$TCARI_{Rb,705}$	-0.41		
$CIRE_{740}$	-0.51	$TCARI_{Rb,740}$	0.66		
$RENDVI_{705}$	-0.76	PRI	0.17		
$RENDVI_{717}$	-0.77	CCI	-0.77		

NDVI: Normalized difference vegetation index; GNDVI: green normalized difference vegetation index; NDRE: normalized difference red edge index; SAVI: soil adjusted vegetation index; OSAVI: optimized soil-adjusted vegetation index; CIgreen: green chlorophyll index; CIRE: red edge chlorophyll index; RENDVI: red edge NDVI; SR: simple ratio; CCCI: canopy chlorophyll content index; MTCI: MERIS terrestrial chlorophyll index; NDWI: normalized difference water index; RVI: ratio vegetation index; TCARI: transformed chlorophyll absorption in reflectance index; PRI: photochemical reflectance index; CCI: canopy chlorophyll content index.

(CWSI) and spectral reflectance (vegetation indices and spectral bands). The results indicate that, for the most part, the spectral bands exhibit a positive correlation, except for the NIR842 (-0.55) and RedEdge740 (-0.43) bands. The Red668 band (0.72) was the only one that met the selection criterion. On the other hand, VIs generally demonstrated better performance. This analysis allowed for the identification of the most suitable variables to correlate with the CWSI, selecting 23 variables (22 VIs and 1 spectral band) with superior performance.

3.4. Comparison of machine learning algorithms performance in estimating water stress

Figure 8 illustrates the comparative evaluation of the performance of algorithms based on the selected VIs and spectral bands obtained from UAV flights. The Random Forest (RF) machine learning algorithm demonstrated the lowest average Root Mean Square Error (RMSE) of 0.13 and Mean Absolute Error (MAE) of 0.09, along with the highest R^2 value of 0.80, positioning it as the best-performing algorithm.

These results align with previous studies, such as that by Yang *et al.* (2021) on Brassica Chinensis, where RF (RMSE = 2.90) outperformed Support Vector Machine (SVM) (RMSE = 3.11) in RMSE analysis. Similarly, Kapari *et al.* (2024) reported superior performance with RF (RMSE = 0.06, MAE = 0.05) compared to SVM (RMSE = 0.09, MAE = 0.06) and Regularized Least Squares (RLS) (RMSE = 0.1, MAE = 0.08) for estimating CWSI in maize, reinforcing the superiority of the RF model for predicting water stress-related parameters.

The second-best performing algorithm was K-Nearest Neighbors (KNN), which exhibited MAE (0.09) and RMSE (0.13) values identical to those of RF but had a slightly lower R^2 value of 0.79. The Gradient Boosting Regressor (GBR) yielded MAE = 0.10, RMSE = 0.14, and R^2 = 0.77, which were slightly lower than those of the previous models.

To identify the relationship or trend between the variables, a scatter plot was constructed using the six best-performing algorithms (Figure 9). This

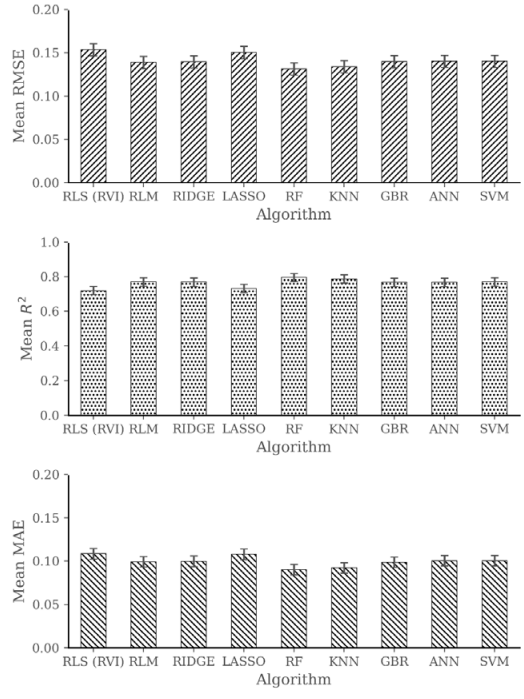

Figure 8. Average root mean squared error (RMSE) (a), coefficient of determination (R2) (b), and mean absolute error (MAE) (c) derived from the use of the following algorithms: Regularized least squares (RLS), multiple linear regression (MLR), ridge regression (RIDGE), least absolute shrinkage and selection operator (LASSO), random forest (RF), K-nearest neighbors (KNN), gradient boosting regressor (GBR), artificial neural networks (ANN), and support vector machines (SVM).

scatter plot presents the predicted CWSI values in comparison to the observed CWSI values, where we can note a higher concentration of data in the ranges of 0.2 to 0.6 and 0.8 to 1. Generally, a strong positive trend is observed, with a clear linear relationship in most cases, except for the Gradient Boosting Regressor (GBR) algorithm. In this case, although the trend is linear, there is a certain grouping resembling columns in the range of 0.4 to 0.6, which introduces some bias when estimating CWSI values, resulting in a lower R^2 compared to the other two models. While the R^2 values indicate that the models explain a good portion of the variability in the data (0.77-0.80), there is also some dispersion, especially in the lower CWSI values, suggesting that the models may struggle to accurately estimate lower CWSI values.

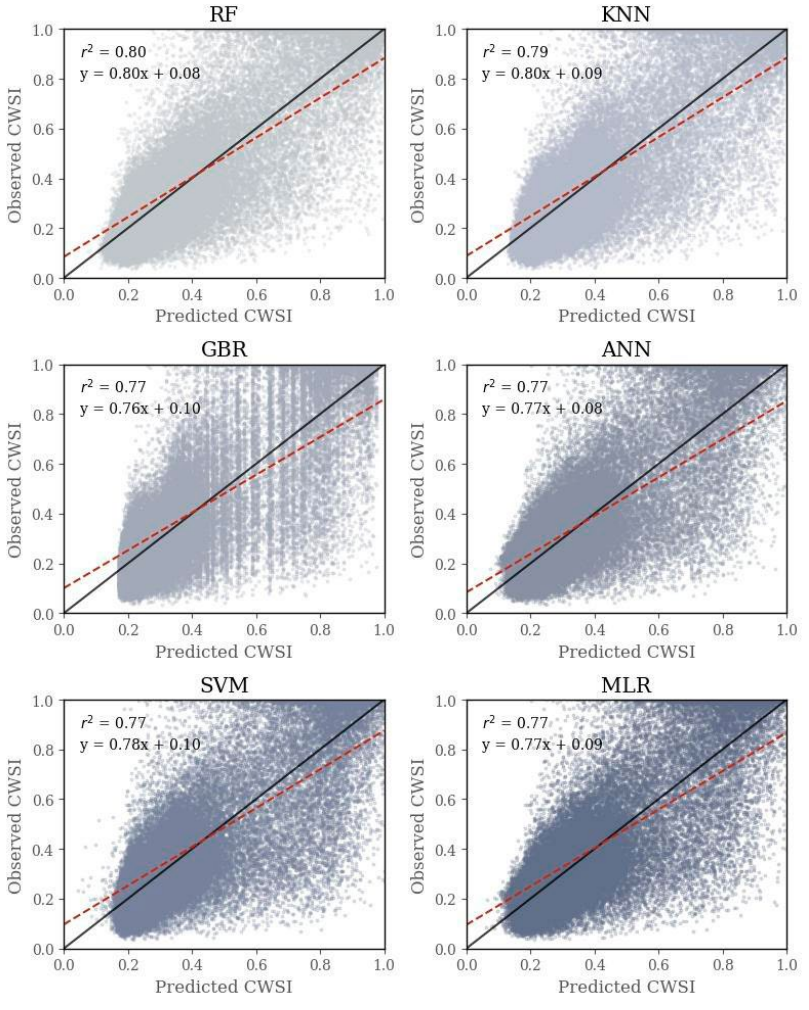

Figure 9. Relationship between observed and predicted CWSI using vegetative indices and spectral bands through machine learning models: Random Forest (RF) (a), K-nearest neighbors (KNN) (b), gradient boosting regression (GBR) (c), Artificial neuronal network (ANN) (d), support vector machine, multiple linear regression (MLR) (e).

The RF model provided the best results, similar to those reported by Kapari *et al.* (2024), due to its tolerance for highly correlated variables (Ma *et al.*, 2021), such as bands alongside vegetation indices. Additionally, it is flexible and suitable for capturing nonlinear relationships. In contrast, the KNN and MLR models exhibited lower performance because they only capture linear relationships and are sensitive to outliers (Pinto *et al.*, 2024). Meanwhile, the GBR and ANN models tend to overfit the training data, making their generalization to new data less accurate (Bhagat *et al.*, 2024).

The red band (650-658 nm) showed a high positive correlation with water stress ($r > 0.68$), indicating its sensitivity to chlorophyll reduction under stress. Although the red-edge band (677-740 nm) is widely associated with chlorophyll, its correlation was lower in this context, possibly due to the marked spectral response of red in advanced stages of stress (Kapari *et al.*, 2025). In addition, vegetation indices incorporating corrections due to soil effect (e.g., SAVI, OSAVI) were used, which also exhibited correlations just as significant as the red band ($r < -0.71$), assuring us that reflectivity values are from vegetation.

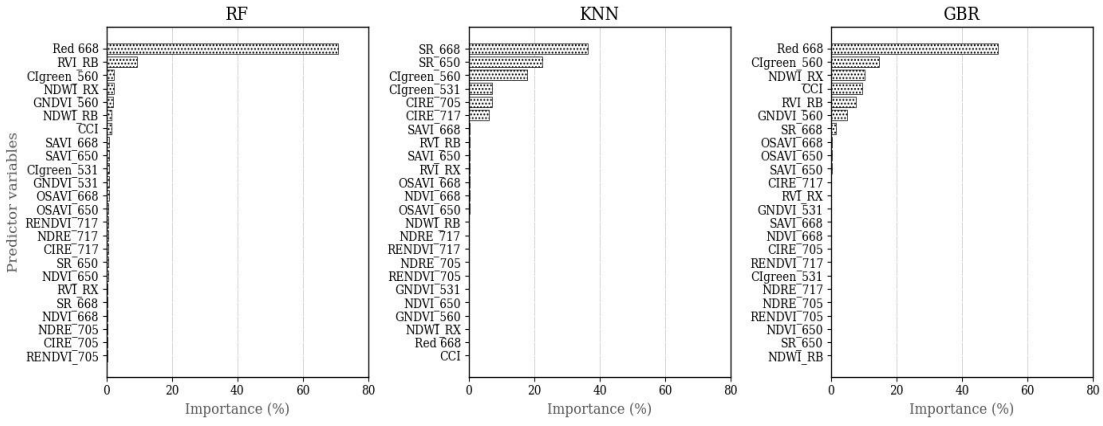

Figure 10. Importance of predictor variables in machine learning models: Random Forest (RF) (a), K-nearest neighbors (KNN) (b), and gradient boosting regressor (GBR) (c).

This fact has been corroborated by studies such as that of Naik *et al.* (2020) and is consistent with the results obtained through the RF and GBR models (Figure 10 a-c), where the red band (668 nm) achieved an importance of 70.69% and 50.92%, respectively. This is attributed to the fact that the water deficit induces physiological and biochemical alterations in plants, resulting in a decrease in photosynthesis and consequently a reduction in chlorophyll content (Gerhards *et al.*, 2018).

In the KNN-based model, the Simple Ratio (SR) index showed the highest level of importance (36.40%). According to Gerhards *et al.* (2016), water stress affects not only the temperature and spectral emissivity of leaves but also the water content, pigment concentration, and the structure of both leaves and the canopy. These changes influence reflectance in the range of solar radiation reflected in the electromagnetic spectrum, making indices like SR optimal for assessing the water status of plants.

3.5. Mapping the spatial distribution of water stress in maize cultivation

The spatial variation of water stress in maize cultivation was modeled using all filtered variables. While the most important variables have a more significant impact on model construction, the others also contribute to improving prediction accuracy. Figure 11 illustrates the spatial variations of water stress (CWSI) across five monitoring dates using the GBR (b), KNN (c), and RF (d) models.

The results indicate that the water stress index varied according to the irrigation conditions applied in the field. Both the RF and KNN models allow for clearer identification of areas affected by water stress, displaying more precise patterns compared to the GBR model, which underestimates CWSI values at 99 days after sowing (DAS). This underestimation may be related to its sensitivity to the nonlinear distribution of data or the influence of less relevant variables on its predictions.

The observed CWSI (Figure 11) at 58 DAS showed a clear distinction between irrigation treatments, with well-watered plots exhibiting significantly lower values (0.0–0.1) compared to stressed plots ($p < 0.001$, ANOVA). While the machine learning models (RF, KNN, GBR) consistently captured significant differences among treatments across all dates ($p < 0.001$ for 35–99 DAS), they exhibited a systematic downward bias in CWSI estimates (0.2–0.3 range). However, the underestimation did not compromise their ability to statistically discriminate treatment effects, as confirmed by the ANOVA results. The narrower dynamic range in model predictions (vs. observations) may reflect the models' conservative response to extreme stress conditions (Su *et al.*, 2020) or residual noise in the input features (Barbedo, 2019).

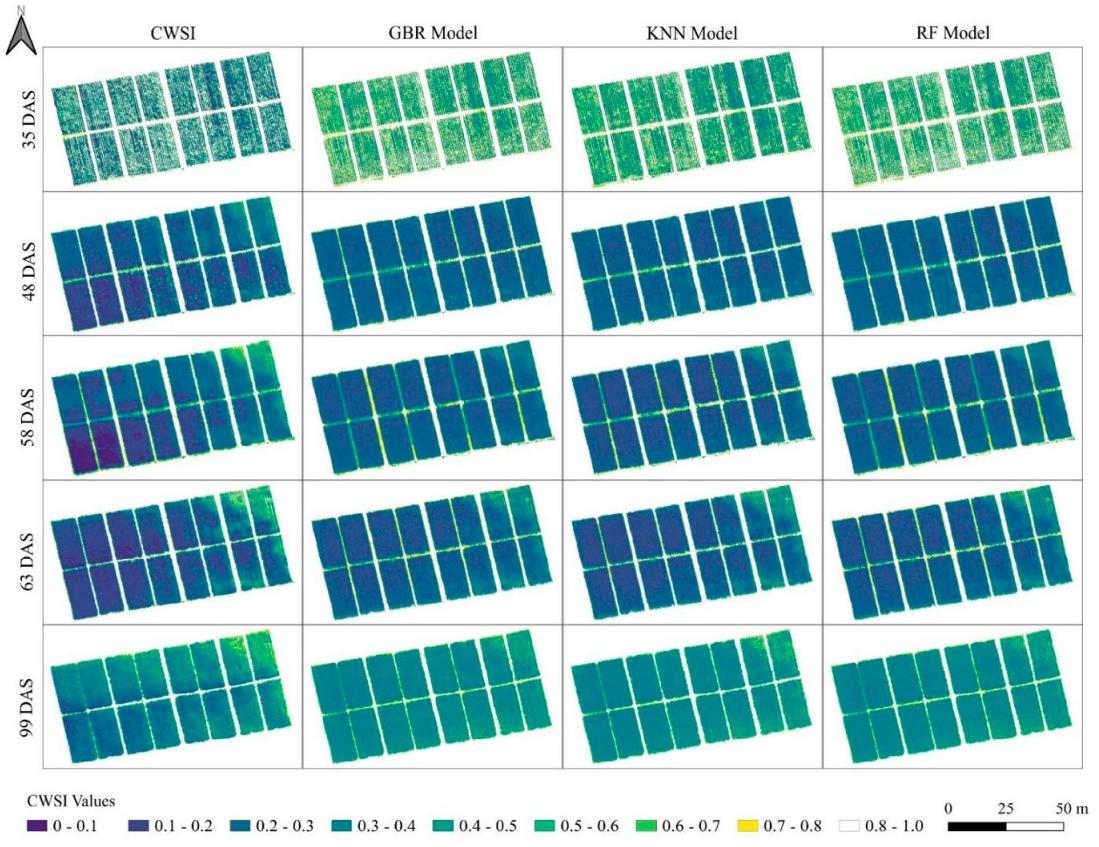

Figure 11. Estimation of the crop water stress index (CWSI) using machine learning algorithms: Gradient boosting regressor (GBR), K-nearest neighbors (KNN), and random forest (RF).

These limitations suggest the need to improve data balancing to avoid underrepresented stress levels, as well as to integrate physiological features that enable the implementation of hybrid models.

4. Conclusions

This study aimed to evaluate the performance of machine learning and regression models in estimating the crop water stress index (CWSI) in maize cultivation, utilizing data collected via UAV in experimental fields. To achieve this goal, different irrigation treatments were applied to generate variability in the data. The results showed that the Random Forest (RF) model was the most suitable for estimating water stress, primarily using the red spectral band (668 nm) as the main variable. This model achieved optimal performance with an R^2 of 0.80, RMSE of 0.13, and MAE of 0.09. Other models, such as K-Nearest Neighbors (KNN) and Gradient Boosting Regressor (GBR), also provided good results.

However, in the spatial and temporal analysis of CWSI, despite satisfactory performance from the algorithms, they tended to overestimate CWSI values calculated from thermal images. Therefore, it is necessary to adjust these models in future campaigns by exploring additional variable combinations and applying hybrid techniques to improve CWSI estimation accuracy. This will enable optimized irrigation management through efficient water resource management using precision agriculture tools.

Acknowledgements

We would like to express our gratitude to the project *"Creation of the Precision Agriculture Service in the Departments of Lambayeque,*

Huancavelica, Ucayali, and San Martín" (CUI-2449640) for its financial support in carrying out this research. We also extend our appreciation to Eng. Alex Augurto for his valuable logistical management during the study and to Valeria Ávila for her support in administrative management. We would especially thanks to Mr. Graviel Terrones, Mrs. María Quintana and Mr. José Diaz for their support in the field activities.

References

Alabi, T.R., Abebe, A.T., Chigeza, G., Fowobaje, K.R. (2022). Estimation of soybean grain yield from multispectral high-resolution UAV data with machine learning models in West Africa. *Remote Sensing Applications: Society and Environment, 27*, 100782. https://doi.org/10.1016/j.rsase.2022.100782

Baluja, J., Diago, M.P., Balda, P., Zorer, R., Meggio, F., Morales, F., Tardaguila, J. (2012). Assessment of vineyard water status variability by thermal and multispectral imagery using an unmanned aerial vehicle (UAV). *Irrigation Science, 30*, 511–522. https://doi.org/10.1007/s00271-012-0382-9

Bannari, A., Morin, D., Bonn, F., Huete, A.R. (1995). A review of vegetation indices. *Remote Sensing Reviews, 13*, 95–120. https://doi.org/10.1080/02757259509532298

Barbedo, J.G.A. (2019). A review on the use of unmanned aerial vehicles and imaging sensors for monitoring and assessing plant stresses. *Drones, 3*(2), 40. https://doi.org/10.3390/drones3020040

Baret, F., Guyot, G. (1991). Potentials and limits of vegetation indices for LAI and APAR assessment. *Remote Sensing of Environment, 35*, 161–173. https://doi.org/10.1016/0034-4257(91)90009-U

Berni, J.A.J., Zarco-Tejada, P.J., Sepulcre-Cantó, G., Fereres, E., Villalobos, F. (2009). Mapping canopy conductance and CWSI in olive orchards using high resolution thermal remote sensing imagery. *Remote Sensing of Environment, 113*, 2380–2388. https://doi.org/10.1016/j.rse.2009.06.018

Bhagat, D., Shah, S., Gupta, R.K. (2024). Crop yield prediction using machine learning approaches. In *International Conference on Machine Learning, Image Processing, Network Security and Data Sciences* (pp. 63–74). Springer Nature. https://doi.org/10.1007/978-3-031-62217-5_6

Daniels, L., Eeckhout, E., Wieme, J., Dejaegher, Y., Audenaert, K., Maes, W.H. (2023). Identifying the optimal radiometric calibration method for UAV-based multispectral imaging. *Remote Sensing, 15*(11), 2909. https://doi.org/10.3390/rs15112909

Dash, J., Curran, P.J. (2004). The MERIS terrestrial chlorophyll index. *International Journal of Remote Sensing, 25*, 5403–5413. https://doi.org/10.1080/0143116042000274015

Del Río, L., Posanski, D., Gracia, F.J., Pérez-Romero, A.M. (2020). A comparative approach of monitoring techniques to assess erosion processes on soft cliffs. *Bulletin of Engineering Geology and the Environment, 79*(4), 1797-1814. https://doi.org/10.1007/s10064-019-01680-2

Duran, M., Ramos, L., Alvarado, R., Altamirano, L. (2021). Evaluation of the crop water stress index (CWSI) in chili pepper (*Capsicum*) under drip irrigation in the arid conditions of the north coast of Peru. *Scientia Agropecuaria.* https://doi.org/10.17268/sci.agropecu.2021.052

Ekinzog, E., Schlerf, M., Kraft, M., Werner, F., Riedel, A., Rock, G., Mallick, K. (2022). Revisiting crop water stress index based on potato field experiments in Northern Germany. *Agricultural Water Management, 269*, 107664. https://doi.org/10.1016/j.agwat.2022.107664

Elsherbiny, O., Zhou, L., Feng, L., Qiu, Z. (2021). Integration of visible and thermal imagery with an artificial neural network approach for robust forecasting of canopy water content in rice. *Remote Sensing, 13*(9), 1785. https://doi.org/10.3390/rs13091785

El-Shikha, D.M., Barnes, E.M., Clarke, T.R., Hunsaker, D.J., Haberland, J.A., Pinter, P.J., Jr., Waller, P.M., Thompson, T.L. (2008). Remote sensing of cotton nitrogen status using the canopy chlorophyll content index (CCCI). *Transactions of the ASABE, 51*(1), 73–82. https://doi.org/10.13031/2013.24228

Feng, A., Zhou, J., Vories, E., Sudduth, K.A. (2020). Evaluation of cotton emergence using UAV-based narrow-band spectral imagery with customized image alignment and stitching algorithms. *Remote Sensing, 12*(11), 1764. https://doi.org/10.3390/rs12111764

Feurer, M., Klein, A., Eggensperger, K., Springenberg, J., Blum, M., Hutter, F. (2015). Efficient and robust automated machine learning. In *Advances in Neural Information Processing Systems* (pp. 2962–2970).

Gamon, J., Serrano, L., Surfus, J.S. (1997). The photochemical reflectance index: An optical indicator of photosynthetic radiation use efficiency across species, functional types, and nutrient levels. *Oecologia, 112*, 492–501. https://doi.org/10.1007/s004420050337

Gerhards, M., Schlerf, M., Rascher, U., Udelhoven, T., Juszczak, R., Alberti, G., Miglietta, F., Inoue, Y. (2018). Analysis of airborne optical and thermal imagery for detection of water stress symptoms. *Remote Sensing, 10*(7), 1139. https://doi.org/10.3390/rs10071139

Gerhards, M., Rock, G., Schlerf, M., Udelhoven, T. (2016). Water stress detection in potato plants using leaf temperature, emissivity, and reflectance. *International Journal of Applied Earth Observation and Geoinformation, 53*, 27–39. https://doi.org/10.1016/j.jag.2016.08.004

Giovos, R., Tassopoulos, D., Kalivas, D., Lougkos, N., Priovolou, A. (2021). Remote sensing vegetation indices in viticulture: A critical review. *Agriculture, 11*, 457. https://doi.org/10.3390/agriculture11050457

Gitelson, A.A., Kaufman, Y.J., Merzlyak, M.N. (1996). Use of a green channel in remote sensing of global vegetation from EOS-MODIS. *Remote Sensing of Environment, 58*(3), 289–298. https://doi.org/10.1016/S0034-4257(96)00072-7

Gitelson, A., Merzlyak, M.N. (1994). Quantitative estimation of chlorophyll-a using reflectance spectra: Experiments with autumn chestnut and maple leaves. *Journal of Photochemistry and Photobiology B: Biology, 22*(3), 247–252. https://doi.org/10.1016/1011-1344(93)06963-4

Haboudane, D., Miller, J.R., Tremblay, N., Zarco-Tejada, P.J., Dextraze, L. (2002). Integrated narrow-band vegetation indices for prediction of crop chlorophyll content for application to precision agriculture. *Remote Sensing of Environment, 81*(2–3), 416–426. https://doi.org/10.1016/S0034-4257(02)00018-4

Han, M., Zhang, H., DeJonge, K.C., Comas, L.H., Trout, T.J. (2016). Estimating maize water stress by standard deviation of canopy temperature in thermal imagery. *Agricultural Water Management, 177*, 400–409. https://doi.org/10.1016/j.agwat.2016.08.031

Hastie, T., Friedman, J., Tibshirani, R. (2001). *The elements of statistical learning*. Springer Series in Statistics. https://doi.org/10.1007/978-0-387-21606-5

Huete, A.R. (1988). A soil-adjusted vegetation index (SAVI). *Remote Sensing of Environment, 25*, 295–309. https://doi.org/10.1016/0034-4257(88)90106-X

Idso, S., Jackson, R., Pinter, P., Reginato, R., Hatfield, J. (1981). Normalizing the stress-degree-day parameter for environmental variability. *Agricultural Meteorology, 24*, 45–55. https://doi.org/10.1016/0002-1571(81)90032-7

Ihuoma, S.O., Madramootoo, C.A. (2017). Recent advances in crop water stress detection. *Computers and Electronics in Agriculture, 141*, 267–275. https://doi.org/10.1016/j.compag.2017.07.026

Jackson, R.D., Reginato, R.J., Idso, S.B. (1977). Wheat canopy temperature: A practical tool for evaluating water requirements. *Water Resources Research, 13*(3), 651–656. https://doi.org/10.1029/WR013i003p00651

Jackson, R.D., Idso, S.B., Reginato, R.J., Pinter, P.J. (1981). Canopy temperature as a crop water stress indicator. *Water Resources Research, 17*(4), 1133–1138. https://doi.org/10.1029/WR017i004p01133

Jamshidi, S., Zand-Parsa, S., Kamgar-Haghighi, A.A., Shahsavar, A.R., Niyogi, D. (2020). Evapotranspiration, crop coefficients, and physiological responses of citrus trees in semi-arid climatic conditions. *Agricultural Water Management, 227*, 105838. https://doi.org/10.1016/j.agwat.2019.105838

Jin, N., Ren, W., Tao, B., He, L., Ren, Q., Li, S., Yu, Q. (2018). Effects of water stress on water use efficiency of irrigated and rainfed wheat in the Loess Plateau, China. *Science of the Total Environment, 642*, 1–11. https://doi.org/10.1016/j.scitotenv.2018.06.028

Jones, H.G. (1999). Use of infrared thermometry for estimation of stomatal conductance as a possible aid to irrigation scheduling. *Agricultural and Forest Meteorology, 95*(3), 139–149. https://doi.org/10.1016/S0168-1923(99)00030-1

Jones, H.G., Leinonen, I. (2003). Thermal imaging for the study of plant water relations. *Journal of Agricultural Meteorology, 59*(3), 205–217. https://doi.org/10.2480/agrmet.59.205

Kapari, M., Sibanda, M., Magidi, J., Mabhaudhi, T., Mpandeli, S., Nhamo, L. (2025). Assessment of the maize crop water stress index (CWSI) using drone-acquired data across different phenological stages. *Drones, 9*(3), 192. https://doi.org/10.3390/drones9030192

Kapari, M., Sibanda, M., Magidi, J., Mabhaudhi, T., Nhamo, L., Mpandeli, S. (2024). Comparing machine learning algorithms for estimating the maize crop water stress index (CWSI) using UAV-acquired remotely sensed data in smallholder croplands. *Drones, 8*(2), 61. https://doi.org/10.3390/drones8020061

Kramer, O. (2016). Scikit-learn. In *Studies in Big Data* (pp. 45–53). Springer. https://doi.org/10.1007/978-3-319-33383-0_5

Li, L., Nielsen, D.C., Yu, Q., Ma, L., Ahuja, L.R. (2010). Evaluating the crop water stress index and its correlation with latent heat and CO2 fluxes over winter wheat and maize in the North China Plain. *Agricultural Water Management, 97*, 1146–1155. https://doi.org/10.1016/j.agwat.2008.09.015

Long, S.P., Ort, D.R. (2010). More than taking the heat: Crops and global change. *Current Opinion in Plant Biology, 13*, 240–247. https://doi.org/10.1016/j.pbi.2010.04.008

Ma, D., Rehman, T.U., Zhang, L., Maki, H., Tuinstra, M.R., Jin, J. (2021). Modeling of diurnal changing patterns in airborne crop remote sensing images. *Remote Sensing, 13*, 1719. https://doi.org/10.3390/rs13091719

Maes, W.H., Steppe, K. (2012). Estimating evapotranspiration and drought stress with ground-based thermal remote sensing in agriculture: a review. *Journal of Experimental Botany, 63*(13), 4671-4712. https://doi.org/10.1093/jxb/ers165

Naik, B.B., Naveen, H.R., Sreenivas, G., et al. (2020). Identification of water and nitrogen stress indicative spectral bands using hyperspectral remote sensing in maize during post-monsoon season. *Journal of the Indian Society of Remote Sensing, 48*, 1787–1795. https://doi.org/10.1007/s12524-020-01200-w

Özelkan, E. (2020). Water body detection analysis using NDWI indices derived from Landsat-8 OLI. *Polish Journal of Environmental Studies, 29*, 1759–1769. https://doi.org/10.15244/pjoes/110447

Peñuelas, J., Gamón, J.A., Griffin, K.L., Field, C.B. (1993). Assessing community type, plant biomass, pigment composition, and photosynthetic efficiency of aquatic vegetation from spectral reflectance. *Remote Sensing of Environment, 46*, 110–118. https://doi.org/10.1016/0034-4257(93)90088-F

Pinto, A.A., Zerbato, C., de Souza Rolim, G.A. (2024). Machine learning models approach and remote sensing to forecast yield in corn with based cumulative growth degree days. *Theoretical and Applied Climatology, 155*, 7285–7294. https://doi.org/10.1007/s00704-024-05071-w

Poblete-Echeverría, C., Espinace, D., Sepúlveda-Reyes, D., Zúñiga, M., Sanchez, M. (2018). Analysis of crop water stress index (CWSI) for estimating stem water potential in grapevines: Comparison between natural reference and baseline approaches. In *VIII International Symposium on Irrigation of Horticultural Crops, 1150*, 189–194. https://doi.org/10.17660/ActaHortic.2017.1150.27

Pradawet, C., Khongdee, N., Pansak, W., Spreer, W., Hilger, T., Cadisch, G. (2022). Thermal imaging for assessment of maize water stress and yield prediction under drought conditions. *Journal of Agronomy and Crop Science, 209*(1), 56–70. https://doi.org/10.1111/jac.12582

Schauberger, B., Archontoulis, S., Arneth, A., Balkovic, J., Ciais, P., Deryng, D., Elliott, J., Folberth, C., Khabarov, N., Müller, C. (2017). Consistent negative response of US crops to high temperatures in observations and crop models. *Nature Communications, 8*, 13931. https://doi.org/10.1038/ncomms13931

Song, L., Jiming, J., Jianqiang, H. (2019). Effects of severe water stress on maize growth processes in the field. *Sustainability, 11*(18), 5086. https://doi.org/10.3390/su11185086

Su, J., Coombes, M., Liu, C., Zhu, Y., Song, X., Fang, S., Guo, L., Chen, W.H. (2020). Machine learning-based crop drought mapping system by UAV remote sensing RGB imagery. *Unmanned Systems, 8*(1), 71–83. https://doi.org/10.1142/S2301385020500053

Ummenhofer, C.C., Meehl, G.A. (2017). Extreme weather and climate events with ecological relevance: A review. *Philosophical Transactions of the Royal Society B: Biological Sciences, 372*(1723), 20160135. https://doi.org/10.1098/rstb.2016.0135

Varco, J.J., Fox, A.A., Raper, T.B., Hubbard, K.J. (2013). Development of sensor-based detection of crop nitrogen status for utilization in variable rate nitrogen fertilization. In *Proceedings of the International Conference on Precision Agriculture* (pp. 145–150). https://doi.org/10.3920/9789086867783_018

Villar, D., Ramos, L., Alminagorta, O. (2021). Evaluación del estrés hídrico del cultivo de arroz (IR 71706) a través del uso de termografía calibrada del área del dosel en Lima, Perú. *Idesia, 39*(4), 59–70. https://doi.org/10.4067/S0718-34292021000400059

Virtanen, P., Gommers, R., Oliphant, T.E., Haberland, M., Reddy, T., et al. (2020). SciPy 1.0: Fundamental algorithms for scientific computing in Python. *Nature Methods, 17*(3), 261–272. https://doi.org/10.1038/s41592-019-0686-2

Wang, X., Li, X., Guo, J., Sun, W., Zhang, H., Chen, S., Yang, S. (2023). Drought and waterlogging status and dominant meteorological factors affecting maize (Zea mays L.) in different growth and development stages in Northeast China. *Agronomy, 13*(2), 374. https://doi.org/10.3390/agronomy13020374

Waqas, M.A., Wang, X., Zafar, S.A., Noor, M.A., Hussain, H.A., Nawaz, M.A., Farooq, M. (2021). Thermal stresses in maize: Effects and management strategies. *Plants, 10*(2), 293. https://doi.org/10.3390/plants10020293

Xue, J., Su, B. (2017). Significant remote sensing vegetation indices: A review of developments and applications. *Journal of Sensors, 2017*, 1353691. https://doi.org/10.1155/2017/1353691

Yang, M., Gao, P., Chen, W., Zhou, P., Sun, D., Xie, J., Lu, J., Wang, W. (2021). Research of Brassica chinensis var. parachinensis under water stress based on machine learning. *Journal of South China Agricultural University, 42*(5), 117–126.

Ying, X. (2019). An overview of overfitting and its solutions. *Journal of Physics: Conference Series, 1168*, 022022. https://doi.org/10.1088/1742-6596/1168/2/022022

Zafar, S.A., Hameed, A., Nawaz, M.A., Wei, M., Noor, M.A., Hussain, M. (2018). Mechanisms and molecular approaches for heat tolerance in rice (Oryza sativa L.) under climate change scenario. *Journal of Integrative Agriculture, 17*, 726–738. https://doi.org/10.1016/S2095-3119(17)61718-0

Zarco-Tejada, P.J., Gonzalez-Dugo, V., Williams, L.E., Suarez, L., Berni, J.A.J., Goldhamer, D., Fereres, E. (2013). A PRI-based water stress index combining structural and chlorophyll effects: Assessment using diurnal narrow-band airborne imagery and the CWSI thermal index. *Remote Sensing of Environment, 138*, 38–50. https://doi.org/10.1016/j.rse.2013.07.024

Zhang, F., Zhou, G. (2015). Estimation of canopy water content by means of hyperspectral indices based on drought stress gradient experiments of maize in the North China Plain. *Remote Sensing, 7*(11), 15203–15223. https://doi.org/10.3390/rs71115203

Zhang, Y., Han, W., Niu, X., Li, G. (2019). Maize crop coefficient estimated from UAV-measured multispectral vegetation indices. *Sensors, 19*(23), 5250. https://doi.org/10.3390/s19235250